ARTICLE

Energetics of topographically designed Smectic-A oily streaks

Amine Missaoui,*[a] Adam L. Susser,[a] Hillel Aharoni,[b] and Charles Rosenblatt[a]

Received 00th January 20xx,
Accepted 00th January 20xx

DOI: 10.1039/x0xx00000x

A thin Smectic-A liquid crystal (LC) film is deposited on a polymer vinyl alcohol-coated substrate that had been scribed with a uniform easy axis pattern over a square of side length L ≤ 85 μm. The small size of the patterned region facilitates material distribution to form either a hill (for a thin film) or divot (for a thick film) above the scribed square and having an oily streak (OS) texture. Optical profilometry measurements vs. film thickness suggest that the OS structure aims to adopt a preferred thickness z_0 that depends on the nature of the molecule, the temperature, and the surface tension at the air interface. We present a phenomenological model that estimates the energy cost of the OS layer as its thickness deviates from z_0.

Introduction

In the Smectic-A (SmA) liquid crystal (LC) phase, molecules are arranged in a lamellar structure with two-dimensional liquid-like order within the lamellae, and where molecular director is oriented on average normal to the lamellae [1]. A "perfect" *SmA* phase, in which the lamellar spacing is constant and the director remains perpendicular to the lamellae, supports splay-like distortions, but not twist or bend. A variety of defect structures may occur, generally involving dislocations in the lamellar structure, as discussed in the book by Kleman and Lavrentovich [2].

In recent years the so-called "oily streak" texture has received great attention [3-17]. The oily streak structure is found when a thin SmA film of thickness d ~1 μm rests on a substrate treated for uniform planar alignment of the director, with the opposing air interface promoting a vertical (homeotropic) boundary condition (Fig. 1). Based on the pioneering X-ray, optical, and atomic force microscopy work of Lacaze's group in Paris [11-16], we understand that, in order to satisfy the competing boundary conditions, the film decomposes into a series of hemicylinders of SmA lamellae with disclination lines running parallel to the hemicylinders and perpendicular to the surface's easy axis; the spatial period is of order 1 to 2 μm. Between disclination lines there typically is a melted (nematic) region near the substrate [13] that facilitates the appropriate anchoring required by the two boundary layers. It is the visible disclination lines that give the structure the whimsical moniker "oily streaks", even though no oil is present. The main structural features, such as hemicylinder periodicity *vs.* film thickness d and the contact angles at the disclinations, have been elucidated [11-16], although these structures have proven to be very challenging to model mathematically. Nevertheless, Xia, et al. have recently developed a free energy functional model for smectic LCs [17]. Using a finite element simulation, their study predicted an energy function for oily streak-type structures in a closed geometry with competing boundary conditions on the top and bottom substrates, but without the free interface that we study here.

In recent work our group examined the topography of a *nematic* LC / air interface above a substrate patterned with a strength s = +1 topological defect [18]. The very large topographical variation relative to the surrounding regions observed above the patterned defect suggests that LC material can be transported over short distances (tens of micrometers) from – or into – the surrounding region in order to minimize the energy of the underlying film. Because *SmA* oily streak experiments have, to date, involved only large area films of uniform thickness, no significant topographical features (other than the relatively small surface crenellations of the hemicylinders [11-16]) have been observed. Therefore, motivated by our nematic film results, we applied an analogous technique to the substrate that underlies the *SmA* film, but in this case we scribed a *uniform* director orientation over a limited area, *i.e.*, no larger than 85 x 85 μm, using an atomic force microscope stylus. These regions are sufficiently small to facilitate transport of LC either into or out of the fully scribed region relative to the surrounding film, with the transport direction dependent on the thickness d of the surrounding unpatterned film. We measured the film topography as a function of d using optical profilometry. Based upon our measurements, we postulate that there is a preferred oily streak film thickness z_0 that causes hills to form above the patterned area if the overall film thickness $d < z_0$, or a divot to form if $d > z_0$. Thus, if the average film thickness d were different from the preferred thickness z_0, there would an energetic cost U_{OS} that varies to leading order as $E_{OS}(z - z_0)^2$, where z is the

[a] Dept. of Physics, Case Western Reserve University, Cleveland, Ohio USA 44122.
[b] Dept. Of Complex Systems, Weizmann Institute of Science, Rehovot, Israel.
* Corresponding author email: axm1593@case.edu.

equilibrium height of the hill or divot above the substrate and E_{OS} is a material-dependent parameter at a given temperature. We present a phenomenological model that describes a competition between surface tension and oily streak layer energy, and from this model determine E_{OS} at room temperature as estimated from measurements of z as a function of d. The parameters E_{os} and z_0 represent additional components useful for the development of a full-blown molecular model for oily streak structures with one free surface.

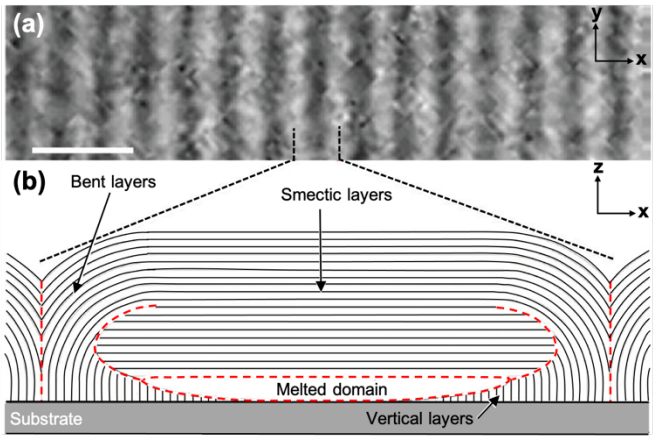

Figure 1: Top: Polarized optical microscopy top view image showing the oily streak pattern between crossed polarizers. Horizontal bar corresponds to 2 μm. Bottom: Side view graphic, based upon the consensus structure developed in Refs. 11-17, showing the SmA layers as well as the formed defects (in red) in oily streaks structure.

Experimental

Microscope glass slides of size 1.5 x 1 cm were sonicated consecutively in detergent dissolved in deionized (DI) water, DI water, acetone, and then ethanol. A thin alignment layer of 3 wt-% polyvinyl alcohol (PVA, Mw = 31000 – 50 000) in DI water was deposited by spin-coating at 3000 rpm for 30 s and then baking at 120 °C for 2 h. The thickness of the PVA film was approximately 70 nm, as described below. To induce planar anchoring conditions, the slides were scribed over a square region of dimensions L x L (L ~ 85 μm) with parallel lines spaced 200 nm apart using AFM nano-lithography [19]. Lines were in alternating directions (*i.e.*, bi-directional = back-and forth) giving rise to near zero pretilt. Outside the scribed PVA region the anchoring was planar random with a small pretilt angle [20-22]. The depth of the grooved lines was ~3 nm. LC in toluene mixtures (concentrations given below) were spin-coated on the PVA coated substrate, resulting in LC films of thicknesses $60 < d < 1500$ nm above the patterned squares. Two LCs were employed: Pure octylcyanobiphenyl (8CB; EM Industries) was used for its room temperature *SmA* phase, while a 60 wt-% mixture of hexylcyanobiphenyl (6CB; EM Industries) in 8CB was used for its room temperature nematic phase; this latter mixture transitions into the *SmA* phase when cooled below room temperature [23]. A mixture of the LCs in toluene with a concentration of 0.01 M was used to create thin LC films, whereas a concentration of 0.5 M was used for thick films. After evaporation of the toluene, an oily streak texture was observed within the patterned square in the *SmA* phase due to competing director boundary conditions at the substrate (planar) and air interface (homeotropic, *i.e.*, vertical orientation) [10-12].

A Zygo NewView 7300 Optical Profilometer was used to measure the topography of the free surface of the LC. The *xy* resolution of the instrument varied between 0.28 and 4.42 μm depending on the objective used, and the z resolution was 0.1 nm.

The thickness of the *SmA* film was determined as follows: First a razor blade was used to scratch the PVA alignment layer down to the glass substrate in a small region far from the scribed square before the LC film was deposited. The optical profilometer was used to determine the depth of the scratch, which corresponds to the thickness of the PVA film. For all samples, the thickness of the PVA was ~70 nm. Next, the LC film was deposited and a razor blade was used to remove a small area of the film near the pattern. The overall thickness of the LC film plus PVA was determined using the optical profilometer by measuring the depth of the removed area with respect to the surrounding. Finally, the thickness of the LC film was deduced from this combined thickness minus the thickness of PVA.

Results and discussion

Let us now turn to our results. We first discuss the behavior of the divots/hills *vs.* time after LC deposition and as a function of square size L; the behavior as a function of film thickness d, which facilitates determination of the preferred divot (hill) depth (height) z_0 and oily streak energetics will be discussed after the theoretical model is introduced. Following deposition of pure 8CB dissolved in toluene, divots or hills formed on the patterned area, depending on the thickness of the *SmA* film. Hills tended to form in thinner films of thickness d ~ 200 nm, while divots formed in thicker films about 800 nm thick (Fig. 2). We shall concentrate on the thick film divots first.

Figure 3a shows the evolution of the depth of a divot in a thick 8CB *SmA* film as a function of temperature. Here L = 85 μm. After deposition at room temperature, the depth of the divot, z - d, was determined to be about -300 nm. Upon heating the initially *SmA* sample (red curve, "heating-1") above the nematic – *SmA* transition, the topography of the patterned area changed from a divot to a hill of about +170 nm in height above d. Then on heating into the isotropic phase, the surface became flat, *i.e.*, the entire LC film became of uniform thickness d. Upon cooling (dark blue curve, "cooling-1") the sample from the isotropic phase, a hill appeared in the nematic phase with a height smaller than that which existed during the first heating. This hill reverted into a divot during the subsequent transition into the *SmA* phase, but was shallower than the original divot observed immediately after the initial deposition. (Note that this work focuses on the *SmA* phase; the behavior of the nematic phase is due to elastic energy considerations [18], and will be examined in more detail elsewhere.)

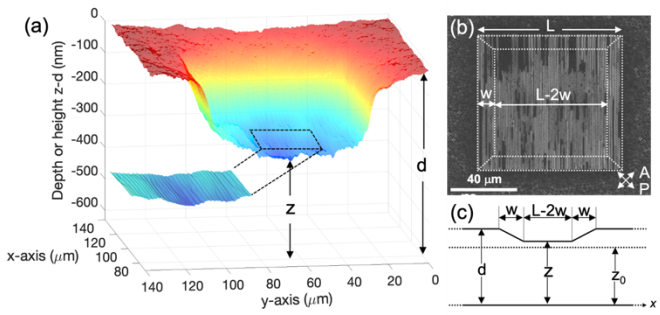

Figure 2: (a) 3D visualization of the rear half of a SmA divot formed above the rubbed PVA as measured using optical profilometry. With enhanced contrast, inset shows the oily streaks. (b) Polarized optical microscopy image showing the OS pattern between crossed polarizers, overlaid by the parameters used in our model below. (c) Side view sketch showing the different parameters in our model used to describe a divot/hill (in this case a divot). The film and OS thickness are defined respectively as d and z. The preferred OS thickness is defined as z_0. The size of the patterned square is L x L and the width (projected into the substrate plane) of the inclined walls is w.

Upon heating and cooling the sample a second time (Fig. 3a, orange and light blue curves, "heating-2" and "cooling-2", respectively), the depth and height of the divot and hill did not vary significantly from cooling-1. The small variation can be attributed to evaporation of the LC, especially during the transition into the isotropic phase, as well as to redistribution of the material in the plane of the film, which can locally change the film thickness.

The fact that the initial depth *z-d* of the divot in thick films decreased after the first heating/cooling cycle and then remained constant thereafter suggests that the initial disorder of *SmA* domains after deposition plays an important role in this phenomenon. More specifically, a thick layer consisting of randomly ordered *SmA* domains would tend to inhibit the formation of the aligned oily streak texture at the substrate. Thus, material would be expelled from the patterned region and the divot would become deeper so that the thinner layer may more easily align and form oily streaks. Once the sample is heated into the nematic phase, the director could become aligned over a larger distance from the substrate, so that a thicker oily streak becomes possible on re-entering the *SmA* phase. Thus, the depth *z-d* of the divot after the first heating would become considerably reduced. This adjustment of *z-d* to an equilibrium depth is the first indication that the oily streak layer likely has a preferred thickness z_0, and which could depend on the particular LC, the temperature, and possibly the anchoring conditions at the alignment layer. To test the idea that the initially deposited *SmA* domains are responsible for the very deep divot, we performed a deposition using the 6CB/8CB mixture, which is nematic at room temperature. Figure 3b shows that when the deposition was performed in the nematic phase, the hill height and divot depth curves remained approximately constant for at least three thermal cycles. Importantly, the initial divot in the *SmA* phase (after cooling from the nematic phase) was considerably shallower than the divot that occurred when the deposition was in the *SmA* phase. This suggests that the smectic disorder is reduced by deposition and surface-induced ordering in the nematic phase, followed by slow cooling into the *SmA* phase and subsequent formation of a thicker oily streak layer.

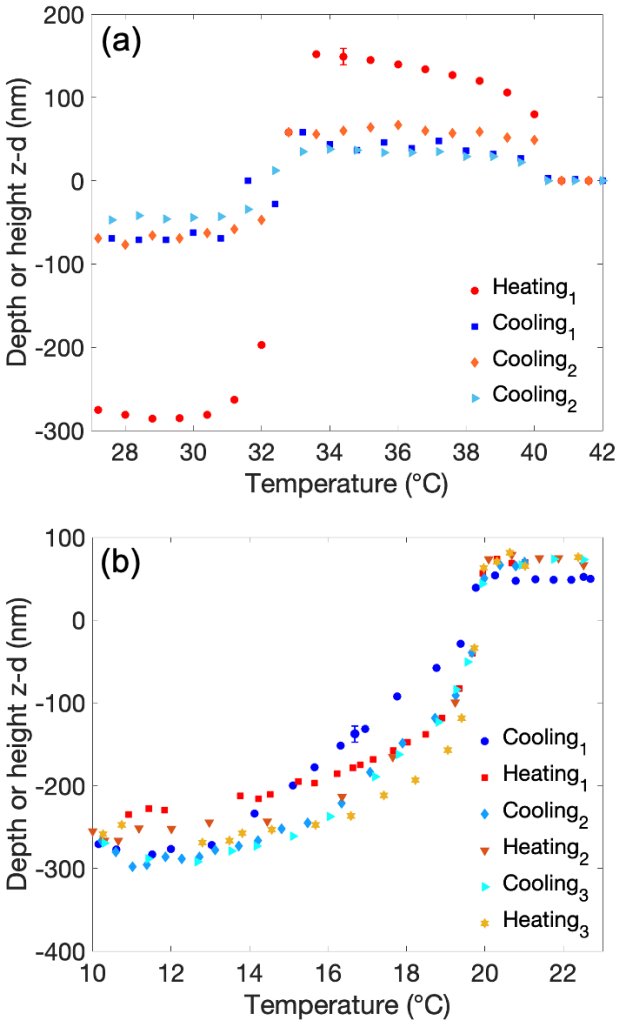

Figure 3: (a) Heat cycling of an 8CB divot. The divot is deep after deposition (red curve) and remains at a reduced constant depth z-d after the first heat cycling. (b) Heat cycle of an 8CB+6CB divot. The LC film was deposited at the nematic phase and then cooled down to the SmA phase. A typical error bar is shown in each.

For thin films, the *SmA* divot / nematic hill phenomenon was reversed: After deposition at room temperature and in the *SmA* phase, a hill was obtained. Moreover, when the sample was heated into the nematic phase, the hill transformed into a divot. Thus, along with the divot in the thick *SmA* film, a hill in the thin film is another indication of a preferred oily streak layer

thickness z_0. This behavior will be a consequence of the phenomenological model developed later in this work.

Figure 4 shows the time evolution of the depth *z-d* relative to the surrounding surface. Four different squares with dimensions *L* x *L* were patterned close to each other on the same substrate. A thick (*d* = 720 nm) 8CB film was then deposited in the *SmA* phase. It is clear that the depth *z-d* increases with the size *L* of the square and decreases with time after deposition. As the disorder of the smectic domains is expected to relax partially over (long) times after the initial deposition, the decrease of the divot depth as a function of time and *without* heating into the nematic phase reinforces the hypothesis that the initial smectic disorder plays an essential role in the large depth *z-d* of the divot immediately after deposition. We remark that anchoring conditions may also change over time, especially in light of the open-air surface, and there could be a small amount of evaporation of LC, although these issues are difficult to quantify.

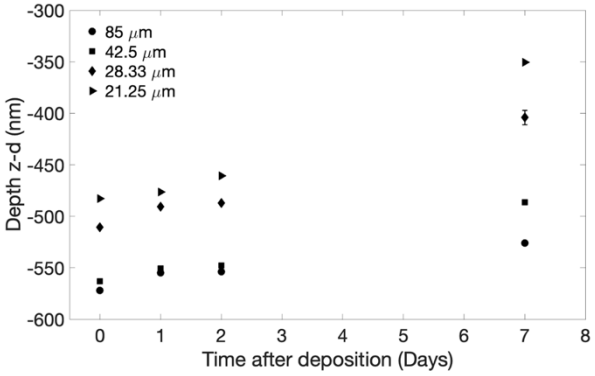

Figure 4: Relaxation over time of 8CB divots for different L at room temperature. Typical error bar is shown.

Although this work focuses on the Smectic-A phase, we turn briefly to the nematic phase, where we observed that the formation of hills and divots depends on the film thickness *d*. For now, we speculate on a possible explanation, although will leave a more detailed examination to future work. Based upon the anchoring conditions inside and outside the scribed region (see above), the director's orientation will vary over approximately 90° (planar to vertical) from the alignment layer to the air interface within the scribed region in thick films, but over a smaller angle outside this region due to the pretilt. This will cause a hill to form over the scribed region so as to extend the 90° reorientation over a larger distance and thereby reduce the energy cost. In thin films, as with thick films, the director outside the scribed region relaxes from the pre-tilted orientation at the interface to the vertical alignment at the air interface. However, in the rubbed region, due to the overall small film thickness, the nematic director cannot perform a full 90° orientational change to build a hill over a great distance, similar to the thick film. As a result, a divot is formed, where we suggest a melted nematic region, *i.e.*, an isotropic phase, *may* appear between the PVA interface and the air interface. [24-25].

We now present a very simple phenomenological model that elucidates the main physical features of the *SmA* films. The model assumes that the hill/divot has reached equilibrium, possibly after multiple thermal cycles. We consider two main contributions to the total energy U_{tot} of the system, viz., $U_{tot} = U_{ST} + U_{OS}$. The first term, U_{ST}, is surface tension energy. We denote by *z(x, y)* the film thickness at every point, and σ is the surface tension energy per area of the LC, which is of the order of ~ 25 erg/cm^2 for 8CB [26]. Then

$$U_{ST} = \iint \sigma\sqrt{1 + |\nabla z|^2}\, dA. \qquad (1)$$

The second term, U_{OS}, is the energy cost due to deviations of oily streak thickness z away from a hypothesized preferred "Goldilocks" thickness z_0. (See Fig. 2) If the overall film thickness *d* just happened to be equal to z_0, then the equilibrium thickness z would also be equal to z_0 and the film would remain flat; this also minimizes U_{ST}. But for most cases $d \neq z_0$. Thus, the actual thickness z would differ from z_0 – being either larger or smaller – and to lowest order there would be an oily streak energy cost U_{OS} given by

$$U_{OS} = \iint \tfrac{1}{2} E_{OS}(z - z_0)^2\, dA. \qquad (2)$$

We note that the quadratic form for the height deviation is only a first approximation. It includes not only an explicit dependence on the local film thickness $z - z_0$, but an implicit dependence on the structure and periodicity of the oily streak, which can vary with $z - z_0$ [8,10,11,13]. Nevertheless, this form reflects the fundamental concept of the phenomenon at work.

Based on experimental observations, we assume that outside of the patterned region the thickness is exactly *d*. These boundary conditions are sufficient to minimize the energy functional $U(z)$ over the patterned region *via* variational calculus. However, to get a better sense of the solution, we further make the phenomenological assumption that, within the scribed region, the height z varies over a constant empirically-determined length scale $w \approx 10\ \mu\text{m}$ (Fig. 2), and remains constant over the central region of the hill or divot of dimensions $(L - 2w) \times (L - 2w)$. These structural features are illustrated in Figure 2. For simplicity, we do not consider the surface crenellations of the oily streak, which are small [7,12]. Using the fact that $|z - d| \ll w$, we obtain $U\_ST \approx \text{const}' + 2\sigma\,(L - w)/w(z - d)^2$ and a somewhat bulky quadratic form in d, z for U_{OS} [See Appendix]. With these we minimize U_{tot} with respect to z. Then, neglecting corrections of order $(w/L)^3$, we get the depth (height) of the divot (hill):

$$z - d = \frac{(L-w)w}{(L-w)w + 4\sigma/E_{OS}}(z_0 - d). \qquad (3)$$

We note that the ratio $(z-d)/(z_0-d) = (L-w)w/((L-w)w + 4\sigma/E_{OS})$ is always between 0 and 1. The model works for hills as well as divots. If the film thickness $d < z_0$, there is a large U_{OS} energy cost unless a hill is created over the patterned region to bring z closer to z_0. And, as with divots, this competes with a surface tension energy due to the hill's lateral surface, resulting in an equilibrium value z such that $d < z < z_0$. Unsurprisingly, we see from Eq. 3 that $z-d$ approaches z_0-d for very large squares where surface tension is negligible, but decreases towards zero as surface tension plays a more prominent role. This result is in qualitative agreement with the dependence of the depth for the square of size L shown in Fig. 4, even though the system in Fig. 4 has yet to reach equilibrium.

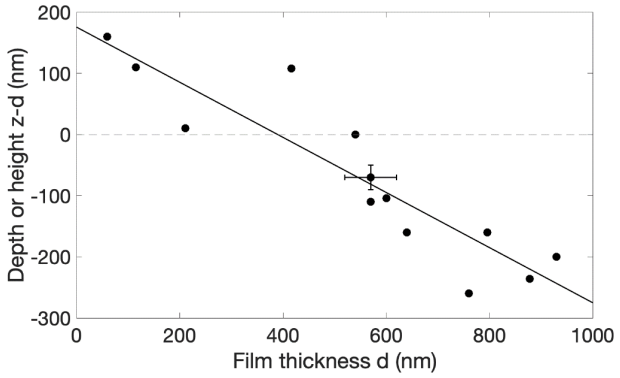

Figure 5: Divot (hill) depth (height) vs. film thickness d for a patterned square of side L = 85 μm. A least-squares fit to Eq. 3 is shown, as are typical error bars. The preferred film thickness z_0 corresponds the crossing point of the fitted line with the z-d = 0 line.

We can use our phenomenological model to study both the natural thickness and the energetics of the oily streaks structure by varying the overall film thickness d. In Eq. 3, the change in depth *z - d vs.* film thickness *d* facilitates extraction of E_{OS} and preferred thickness z_0 if *L*, *w*, and σ are known. In Figure 5 we show the measured depth *vs.* film thickness for several *SmA* samples with patterned regions of size $L = 85$ μm. From a linear fit using Eq. 3 we obtain the "Goldilocks" thickness of the oily streaks, $z_0 = 0.39 \pm 0.15$ μm, and an approximate value (due to the significant scatter in the data) of the energy coefficient for deviations from this thickness, $E_{OS} = (1.2 \pm 0.6) \times 10^{-9} erg\ \mu m^{-4}$. To be sure, these values apply only to 8CB at 25°C. Moreover, our model does not account for the complex structure of the oily streak structure, which both experimentally [11-16] and theoretically [17] has been shown to be a function of film thickness. Nevertheless, with these caveats, it gives us an estimate for the energetics of oily streaks with one free surface.

Conclusions

We have demonstrated a proof-of-concept for controllable manipulation of the free surface topography of a thin *SmA* film for deformations both out of and into the film. For *SmA* films the physics is based on surface tension and the hybrid surface boundary conditions resulting in oily streaks, whereas for nematics the topography is based on surface anchoring and elasticity [18]. Formation of divots in thicker *SmA* films or hills in thinner films occurs because the oily streak layer has a preferred thickness z_0, such that thickness deviations from z_0 entail an energy cost. By examining the topography of this structure, a simple model that includes surface tension allows us to estimate the energetic cost of oily streak layer thickness deviations from the preferred thickness z_0. It is important to note that our small patterned regions facilitate this measurement, as the surrounding unpatterned region serves as a reservoir from which to draw, or into which to deposit, LC material. This is not possible in a large area film of uniform surface treatment. Our results suggest that although oily streaks can form over a large range of *SmA* layer thicknesses [11-16], there is one temperature-dependent special thickness z_0 for a given liquid crystal molecule that the system aims to achieve. If $d \neq z_0$ there will be a strain-like energy cost.

Conflicts of interest

There are no conflicts to declare.

Acknowledgements

We thank Dr. Andrew J. Ferris for useful discussions. CR thanks the Weizmann Institute of Science, Rehovot, Israel for a Weston Visiting Professorship. This work was supported by the National Science Foundation under grant DMR1901797, by the National Aeronautics and Space Administration under grant NNX17AC76G, and the United States-Israel Binational Science Foundation (BSF) under grant 2018380.

Appendix

Outside the scribed region of size $L \times L$, the height is constant $z(x,y) = d$. Inside an inner region of size $(L-2w) \times (L-2w)$, the height is again constant $z(x,y) = z$. In between, we assume that the height changes linearly with the distance from the boundary, namely

$$z(x,y) \approx d + \frac{z-d}{w} \min(\{x, L-x, y, L-y\}).$$

With this, there is a region of area $L^2 - (L-2w)^2$ in between the inner square and outer square in which $|\nabla z| = \left|\frac{z-d}{w}\right|$, and otherwise $|\nabla z| = 0$. Therefore,

$$U_{ST} = \iint \sigma\sqrt{1+|\nabla z|^2}\, dA$$
$$= \text{const} + \sigma(L^2-(L-2w)^2)\sqrt{1+\left|\frac{z-d}{w}\right|^2}$$
$$= \text{const} + 2\sigma\frac{L-w}{w}(z-d)^2 + O[z-d^3].$$

With the same assumption on $z(x,y)$,

$$U_{OS} = \iint \tfrac{1}{2}E_{OS}(z-z_0)^2\, dA$$
$$= \text{const}$$
$$+ \tfrac{1}{2}E_{OS}\left[(L-2w)^2(z-z_0)^2\right.$$
$$\left. + 4\int_0^w (L-2x)\left(d+\frac{x}{w}(z-d)-z_0\right)^2 dx\right]$$
$$= \text{const} + \tfrac{1}{2}E_{OS}\begin{pmatrix} z-d \\ z_0-d\end{pmatrix}^T$$
$$\cdot\begin{pmatrix} L^2-\frac{8Lw}{3}+2w^2 & -L^2+2Lw-\frac{4w^2}{3} \\ -L^2+2Lw-\frac{4w^2}{3} & L^2\end{pmatrix}$$
$$\cdot\begin{pmatrix} z-d \\ z_0-d\end{pmatrix}.$$

Therefore, the total energy of the system takes the form

$$U = \text{const} + \begin{pmatrix} z-d \\ z_0-d\end{pmatrix}^T \cdot M \cdot \begin{pmatrix} z-d \\ z_0-d\end{pmatrix}.$$

The depth at the minimizer satisfies

$$\frac{z-d}{z_0-d} = -\frac{M_{12}}{M_{11}} = \frac{\left(L^2-2Lw+\frac{4}{3}w^2\right)}{\left(L^2-\frac{8}{3}Lw+2w^2\right)+4\frac{L-w}{w}\frac{\sigma}{E_{os}}}$$
$$= \frac{w(L-w)+\frac{w^2}{3}\frac{w}{L-w}}{w(L-w)-\frac{w^2}{3}\left(2-\frac{w}{L-w}\right)+4\frac{\sigma}{E_{os}}}$$
$$= \frac{w(L-w)}{w(L-w)+4\,\sigma/E_{os}} + O\left[\left(\frac{w}{L}\right)^3\right]$$

When discussing large enough squares with respect to the boundary's width, as in the cases described in the paper, the $O\left[\left(\frac{w}{L}\right)^3\right]$ term can be neglected.

References

1 P.G. de Gennes, and J. Prost, The Physics of Liquid Crystals, Clarendon Press, 1993.
2 M. Kleman, and O. Lavrentovich, Springer Science & Business Media, 2003, 637.
3 O. Lehmann, Z. Physikalische Chemie, 1889, **4**, 462.
4 F. Reinitzer, Monatshefte für Chemie, 1888, **9**, 421.
5 G. Friedel, Annales de Physique, 1922, **18**, 273.
6 P. Boltenhagen, O. Lavrentovich and M. Kleman, J. Phys. II., 1991, **1**, 1233.
7 I. R. Nemitz, A. J. Ferris, E. Lacaze, and C. Rosenblatt, Soft Matt.,2016, **12**, 6662.
8 D. Coursault, B. H. Ibrahim, L. Pelliser, B. Zappone, A. de Martino, E. Lacaze, and B. Gallas, Optics Exp., 2014, **22**, 23182.
9 I. Gharbi, A. Missaoui, D. Demaille, E. Lacaze and C. Rosenblatt, Crystals, 2017, **12**, 358.
10 B. Zappone and E. Lacaze, Phys. Rev. E, 2008, **78**, 061704.
11 J. P. Michel, E. Lacaze, M. Alba, M. de Boissieu, M. Gailhanou, and M. Goldmann, Phys. Rev. E, 2004, **70**, 011709.
12 E. Lacaze, J. P. Michel, M. Alba, and M. Goldmann, Phys. Rev. E, 2007, **76**, 041702.
13 D. Coursault, et al., Soft Matt., 2016, **12**, 678.
14 S. P. Do, et al., Nano Lett., 2020, **20**, 1598–1606.
15 S. P. Do, Composites cristaux liquids/nanoparticules, synergies entre matière molle et propriétés électroniques de nanoparticules. Matériaux. Sorbonne Université, 2019.
16 H. Jeridi, et al., Soft Matt., 2022, **25**, 4792-4802.
17 J. Xia, S. MacLachlan, T. J. Atherton, and P. E. Farrell. Phys. Rev. Lett., 2021, **126**, 177801.
18 A. J. Ferris, C. Rosenblatt, and T. J. Atherton, Phys. Rev. Lett., 2021, **126**, 057803.
19 K. E. Vaughn, M. Sousa, D. Kang, and C. Rosenblatt, Appl. Phys. Lett., 2007, **90**, 194102.
20 X. Wei, S. C. Hong, X. Zhuang, T. Goto, and Y. R. Shen, Phys. Rev. E, 2000, **62**, 5160.
21 R. Moldovan, S. Frunză, T. Beica, and G. Barbero, Mol. Cryst. and Liq. Cryst., 2006, **257**, 125.
22 K. Ha, and J. L. West, Liq. Cryst., 2004, **31**, 753.
23 M. Okumus, and S. Özgan, Asian J. of Chem., 2013, **25**, 3879.
24 R. Wang, et al., Phys. Rev. Lett., 2006, **97**, 167802.
25 P. G. de Gennes, Solid State Communications, 1972, **10**.
26 H. Schüring, and R. Stannarius, Liq. Cryst., 2001, **28**, 241.